Lifetime Prediction and Design of Reliability Tests for High-Power Devices in Automotive Applications

Mauro Ciappa, *Senior Member, IEEE*, Flavio Carbognani, and Wolfgang Fichtner, *Fellow, IEEE*

Abstract—Different procedures are defined and compared to extract the statistical distribution of the thermal cycles experienced by power devices that are installed in hybrid vehicles and operated according to arbitrary mission profiles. This enables both to design efficient accelerated tests tailored on realistic data and to provide the input for lifetime prediction models. Initially, the system lifetime is predicted under the assumption of linear accumulation of the damage produced by low cycling fatigue. Also, a novel prediction model based on some fundamental equations is introduced which takes into consideration the creep experienced by compliant materials when they are submitted to thermal cycles.

Index Terms—Automotive electronics, hybrid vehicles, lifetime prediction, power devices.
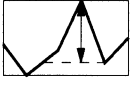
I. INTRODUCTION

THE end-of-life period of complex multichip modules is often defined by thermomechanics-related failure mechanisms. The time-to-failure (lifetime) for these wear-out mechanisms is normally estimated on the basis of deterministic models, which are calibrated with data extracted from accelerated power cycling experiments. Furthermore, these estimates are referred to a given application profile, which is specific to the technical system under consideration (hybrid car, locomotive, etc.). Simple lifetime prediction models, based on the bimetallic approximation for the thermomechanical stresses, and based on principle of the linear accumulation of the damage related to cyclic fatigue, have been proposed and investigated in the past [1], [2], [6]. The main issue about these models is the procedure to define and extract the number, the amplitude, and the duration of the thermal cycles which are experienced by the system when it is submitted to a given mission profile. In the first part of this paper, we shall propose different procedures to extract the statistical distribution of the thermal cycles, and we shall compare and discuss the lifetimes predicted with them. In the second part of the paper, we shall propose a novel prediction procedure, which is based on some fundamental equations of the thermomechanics and takes into consideration the creep suffered by compliant materials when they are submitted to thermal cycles.

TABLE I
SUMMARY OF THE DIFFERENT CYCLE DEFINITIONS

A. Linear Accumulation of the Cyclic Fatigue Damage

Under the hypothesis of linear accumulation of the cyclic fatigue damage, the cumulated fatigue function [1] can be defined as

$$Q = \frac{N(\Delta T)}{N_f(\Delta T)} \quad (1)$$

where N is the number of cycles performed at a given thermal excursion ΔT and N_f is the number of cycles to failure at the same ΔT, respectively.

Differentiation and integration (under the accumulation hypothesis) of Q over a complete mission temperature profile yields [1]

$$Q(\text{after 1 Mission}) = \frac{1}{a} \int_{\Delta T \min}^{\Delta T \max} \frac{g(\Delta T)}{\Delta T^{-q}} d(\Delta T) \quad (2)$$

where $g(\Delta T)$ represents the frequencies distribution of the thermal excursions inside one mission profile. In (2), we have already considered the power-function dependence of N_f on ΔT (Coffin–Manson law), expressed by the coefficient a and the exponent q, which are extracted from accelerated tests (power cycles), and which are assumed as known. Thus, the only unknown quantity in (2) is the function $g(\Delta T)$. The fraction $1/Q$ returns the lifetime prediction expressed in number of mission profiles to failure.

II. THERMAL CYCLE DEFINITIONS

The thermal cycle, whose identification is necessary to extract the $g(\Delta T)$ function, is completely defined through the in-

dication of a time duration and a thermal excursion. Four different definitions are presented below, which can be easily implemented with the usual data processing tools. Table I summarizes Definition A–D in graphical form.

Definition A: Definition A is self-evident. The thermal cycle (and thus its duration) is defined as the interval between two subsequent relative minima. The thermal excursion is assumed to be the difference between the maximum and the minimum temperature within a cycle duration.

Definition B: Definition B is also self-evident. The thermal cycle (and thus its duration) is defined as the interval between two subsequent relative minima. The thermal excursion is assumed to be the difference between the maximum temperature and the temperature at the highest relative minimum within a cycle duration.

Definition C: In Definition C, the thermal cycle (and thus its duration) is defined as the interval between two subsequent relative extremes (inversion points of the derivative). The thermal excursion is assumed to be the difference between the maximum and the minimum temperature within a cycle duration. This definition considers as a full cycle the rising edge and as a subsequent full cycle the falling edge. Thus, it provides a number of cycles, which is doubled compared with Definitions A and B (i.e., it includes all the excursions due to Definition A and B). In spite of the fact that it is well defined, the cycle duration has no physical meaning.

Definition D: In Definition D, the thermal cycle (and thus its duration) is defined as the interval between two subsequent relative minima. The thermal excursion is assumed to be the same as for Definition B with an additional correcting factor Δ computed according to

$$N_f(\Delta) = 2N_f(\Delta T_A - \Delta T_B)$$

where ΔT_A is the thermal excursion according to Definition A and ΔT_B is the thermal excursion according to Definition B. The correction factor Δ aims to compensate the fact that Definition A leads to overestimated excursions, while Definition B to underestimated excursions.

Definition E: This is a simplified version of Definition D. Instead of using the correction factor weighted by the nonlinear Coffin–Manson dependence, we assume here a linear correction expressed by

$$\Delta = 0.5(\Delta T_A - \Delta T_B).$$

This definition greatly simplifies the numerical computations and does not require previous knowledge of the Coffin–Manson parameters a and q.

III. DATA PREPROCESSING

Filtration and truncation procedures are used to quantify the impact of thermal cycles of small amplitude on the predicted lifetime. This low-ΔT cycle tail is often due to measurement noise while acquiring the temperature profiles. In this case, these artifacts have to be suppressed by appropriate data preprocessing.
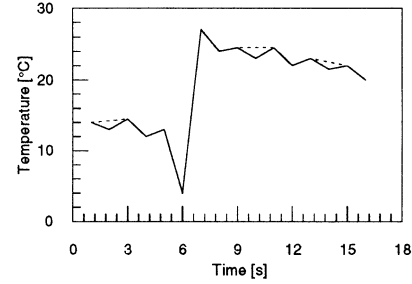

Fig. 1. Junction temperature profile (solid line). The dashed segments represent the smoothing due to the filtration.
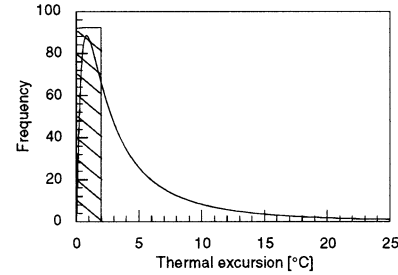

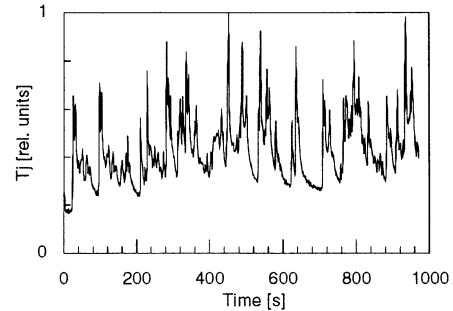Fig. 2. $g(\Delta T)$ after truncation of the dashed interval.

Fig. 3. Time evolution of the junction temperature of an IGBT of a hybrid car operated in an urban environment.

A. Data Filtration

The principle of the filtration procedure used here is drawn in Fig. 1. It is applied directly on the mission profile in such a way that the thermal cycles, where the thermal excursion according to Definition A does not exceed 2°C, are smoothed out.

B. Spectrum Truncation

The truncation procedure is represented in Fig. 2. It is applied to the distribution of the thermal excursion in such a way that thermal cycles whose excursion is smaller than 2°C are not considered in the statistics. In other words, the truncation procedure leads to the suppression of the low-temperature tail of $g(\Delta T)$.

IV. EXTRACTION PROCEDURES

After assuming a given definition for the thermal excursion and a suitable procedure for processing the data (filtration or truncation), the stress model is extracted from an experimental junction temperature profile, as it is plotted in Fig. 3.

This represents the evolution of the junction temperature of an insulated gate bipolar transistor (IGBT) device in a power module, operated within a hybrid car, which is driven according
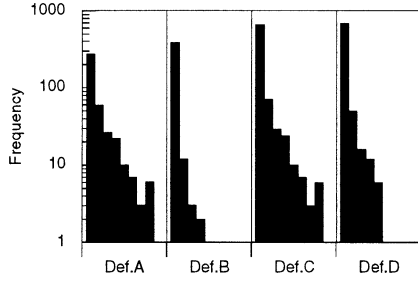
Fig. 4. Frequencies distributions (one slot is 5°C) of ΔT as calculated from the mission profile of Fig. 3.
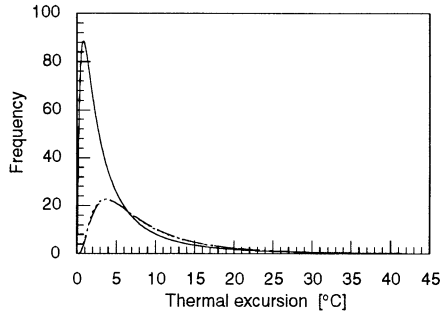

Fig. 5. Lognormal fit of ΔT as calculated from the mission profile of Fig. 3 according to Definition A. Solid: raw, dashed: filtered, dotted: truncated data.
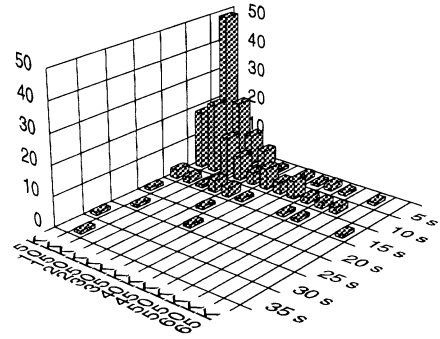

Fig. 6. Frequency of the cycles from Fig. 3 as a function of the cycle excursion and cycle duration with Definition A.

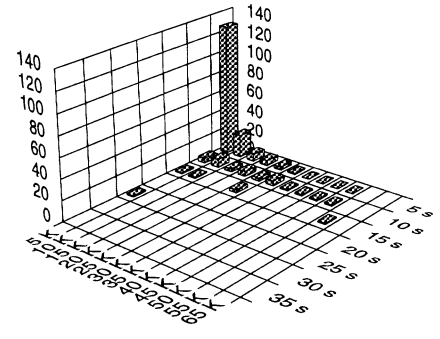Fig. 7. Frequency of the cycles from Fig. 3 as a function of the cycle excursion and cycle duration with Definition A.

to a standard mission profile in an urban environment. In spite of the fact that the junction temperature has been acquired with a sampling period of 500 ms, these data represent a reasonable estimate of the real junction temperature. In fact, the junction temperature increase due to power dissipation spikes (e.g., switching losses) whose duration is much shorter than the typical thermal time constant of the whole system (typically several seconds) is almost negligible. The extracted $g(\Delta T)$ function can be either analytical or numerical. The analytical form can be obtained by fitting the empirical distribution with the usual statistical distributions, i.e., Normal, Lognormal, or Weibull. In general, the best fit is provided by the Lognormal distribution.

The numerical form of $g(\Delta T)$ is represented either by the density of the empirical function as a histogram, or as, it is the case for discrete data, by a series of Dirac distributions on the thermal excursion axis. In this case (2) becomes

$$Q = \sum_j \frac{n_j}{a} \cdot \int_{\Delta T_{\mathrm{MIN}}}^{\Delta T_{\mathrm{MAX}}} \frac{\delta(\Delta T - \Delta T_j)}{\Delta T^{-q}} d(\Delta T) \qquad (3)$$

hence

$$Q = \sum_j \frac{n_j}{a} \cdot \frac{1}{\Delta T_j^{-q}}. \qquad (4)$$

In (4), n_j is the number of thermal cycles extracted from the mission profile at the value ΔT_j. The distribution of the frequency of ΔT, as extracted with Definition A–D, is represented in Fig. 4.

Fig. 5 represents the frequency of the thermal cycles (Definition A) as extracted in analytical form from the mission profile

of Fig. 3 before and after filtration and truncation, respectively. It can be seen that both the truncation and the filtration process lead to a similar result.

V. DESIGN OF RELIABILITY TESTS

The junction temperature is one of the most important parameters for the design of reliability tests for power devices. Thermal and power cycle tests are both performed with the junction temperature of the device under test as a control parameter. Due to the relevance of stress-relaxation phenomena in thermomechanically activated failure mechanisms, the junction temperature alone (or eventually the junction temperature swing) is not sufficient to replicate the stresses and the degradation occurring for a given application profile. In order to take these effects into consideration, every thermal cycle has to be associated to its cycle duration, and eventually to its average baseline temperature (not considered here). This implies a multidimensional statistical analysis. Fig. 6 represents the frequency of the thermal cycles occurring in the standard application profile of Fig. 3, in conjunction with the related cycle duration. Both values have been computed according to Definition A. The raw data have been preprocessed to filter out high-frequency noise and represented as a histogram where every bin covers a temperature span of 5 K and a time interval of 5 s. This representation has been selected to enable an easy implementation of a reliability test. In Fig. 6, it can be observed that the highest bin corresponds to thermal cycles having a temperature swing lower than 5 K and a duration shorter than 5 s. About 80% of the temperature swings are lower than 25 K, while their duration does not exceed 15 s.

The observed maximum temperature swing is 65 K, the maximum cycle duration is 35 s, and the total number of cycles is 206 (for a driving period of 1000 s).

The same statistical analysis has been performed for Definition B and is represented in Fig. 7. Of course, in this case both the average temperature swing and the average cycle duration are smaller than for Definition A. The observed maximum temperature swing is 55 K, the maximum cycle duration is 25 s, and the total number of cycles is the same as before.

VI. New Lifetime Prediction Model Based on the Creep Behavior of the Solder Layer

In order to overcome the problems involved with the arbitrary definition of the thermal cycle, we propose here a prediction model, which makes use of the fundamental thermomechanical equations describing the creep mechanics in materials submitted to cyclic loads [3], [4]. In particular, the proposed model assumes that stresses above the yield point cause a plastic irreversible deformation, which turns into a hysteresis loop in the stress-strain representation.

A. Thermomechanical Models

The uniaxial strain is computed from the thermal expansion of the bimetallic system, while the corresponding shear stress is derived from the creep relation. Once represented in the stress-strain plane, these values provide the deformation energy dissipated during a thermal cycle of arbitrary shape. In fact, it can be easily demonstrated that the deformation energy is proportional to the area included within the corresponding hysteresis loop [4]. The lifetime of the system can be computed under the assumption that the system reaches its end-of-life as soon as a total amount of deformation work (W_{tot}) has been accumulated. Thus, the lifetime of the system (expressed in number of mission profiles) can be computed by calculating the ratio between W_{tot} and the deformation work associated with a given mission profile.

Based on these principles, we propose two different models for the creep behavior of solder materials. The first model includes only the dependency of the shear stress on the temperature gradient and can be summarized by the following equations:

$$\gamma(i) = (T(i) - T_0) \cdot \Delta\alpha \tag{5}$$

$$\tau(i) = \text{sgn}\left(\gamma(i) - \gamma(i-1)\right) \frac{G}{A^{\frac{1}{n}}}$$
$$\cdot \left(\frac{\text{abs}\left(\gamma(i) - \gamma(i-1)\right)}{t_{\text{slot}}}\right)^{\frac{1}{n}} \tag{6}$$

where γ is the shear strain, τ is the shear stress, $\Delta\alpha$ is the mismatch in the thermal expansion coefficients of the layers, which are joined by the solder, and t_{slot} is the time discretizing unit. T is the instantaneous temperature (as sampled from the plot in Fig. 3) and T_0 is the temperature for which the strain is zero. Finally, G, A, and n are parameters that depend on the materials and on the geometry of the system. The second model [(5) and (7)] also takes into account the dependency of the creep
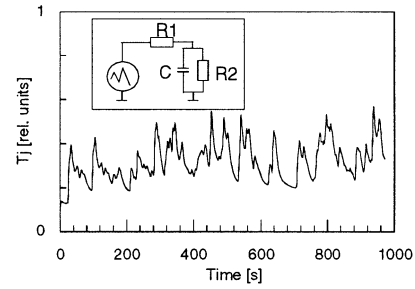

Fig. 8. Temperature on the solder between the base plate and the ceramic insulator from the mission profile in Fig. 3. The insert shows schematically the compact thermal model.

behavior on the instantaneous temperature. This dependency is represented in (7) by the Arrhenius term

$$\tau(i) = \text{sgn}\left(\gamma(i) - \gamma(i-1)\right) \frac{G}{A^{\frac{1}{n}}}$$
$$\cdot \left(\frac{\text{abs}\left(\gamma(i) - \gamma(i-1)\right)}{t_{\text{slot}}} \exp\left(\frac{E_a}{kT(i)}\right)\right)^{\frac{1}{n}} \tag{7}$$

where E_a is the activation energy and k is the Boltzmann constant. All equations are already expressed in their discretized form to enable straightforward numerical computation.

B. Thermoelectrical Compact Model

Before calculating the shear strain and the shear stress with (5), (6), and (7), it is necessary to determine the real temperature profile at the location of the compliant layer under investigation. Since in our case we consider the solder layer between the baseplate and the ceramic insulation layer, we have to take into account the low-pass filtering action provided by the package and by the heat sink. For this scope we compute the local temperature profile basing on a compact thermal model of the device, which has been extracted by thermal simulation [5] and which is schematically represented in the insert of Fig. 8. The resulting temperature profile is shown in Fig. 8.

C. Calibration of the Thermomechanical Models

The aim of the calibration procedure is to determine the value of the parameters n and E_a in (6) and (7) from a set of experimental data (power cycles). The parameters A and G are irrelevant because they are only multiplicative constants. If we assume that the results of the accelerated tests return a function h, which relates the maximum number of allowable thermal cycles to the thermal excursion ΔT, we can extract the required parameters by the least-squares technique. The quantity to be minimized is

$$\xi = \sum_j \left(\frac{W_{\text{tot}}}{W(\Delta T_j, n, E_a)} - h(\Delta T_j)\right)^2 \tag{8}$$

where $W(\Delta T_j, n, E_a)$ is the deformation work due to a single power cycle. This can be computed after having determined the local temperature profile on the solder layer related to the single power cycle (Fig. 9).
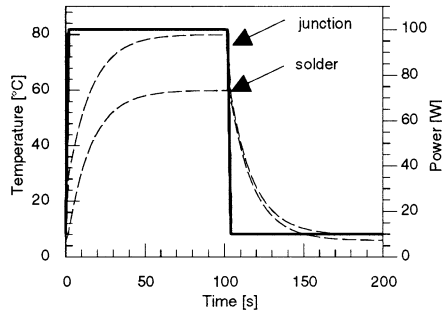
Fig. 9. Step thermal response of the junction versus the solder (see also Fig. 8).
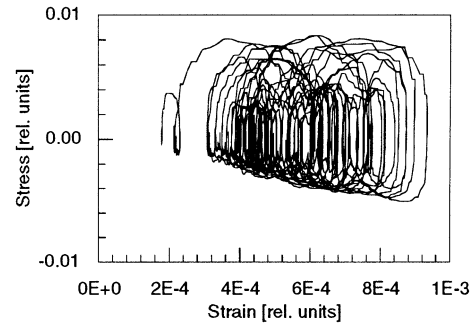

Fig. 10. Stress-strain plot for the mission profile of Fig. 3.

To this purpose we use again the compact thermal model represented schematically in the insert of Fig. 8. In case that the function h is a power function (Coffin–Manson, factor a, exponent q), the parameter E_a reduces to zero. In fact, the number of cycles to failure predicted from the second model is proportional to the reciprocal of the product between (5) and (7), hence to the factor w

$$w = (\Delta T)^{(-1+\frac{1}{n})} \exp\left(-\frac{E_a}{nkT}\right).$$ (9)

When comparing (9) to the Coffin–Manson law, which depends only on the thermal excursion and not on the instantaneous value of the temperature, it is clear that the second term of (9) has to be a constant, i.e., E_a must be zero. Therefore, after differentiation of (8) on W_{tot}, setting it to zero, and solving for W_{tot}, one obtains

$$W_{\text{tot}} = \frac{\sum_j \dfrac{h(\Delta T_j)}{W(\Delta T_j, n)}}{\sum_j \dfrac{1}{W^2(\Delta T_j, n)}}.$$ (10)

In the case that the function h is a pure power law (Coffin–Manson), the insertion of (10) into (8) leads to a one-parameter fit procedure to extract n. In the most general case, the problem requires a two-parameters fit procedure for n and E_a.

D. Lifetime Prediction According to the New Model

Once calibrated, the model applied to the mission profile of Fig. 3 returns the instantaneous stress-strain values, which are plotted with the time as a parameter in Fig. 10. The area enclosed within every single loop represents the total plastic deformation work associated with the mission profile.

VII. COMPARISON OF LIFETIME PREDICTIONS AMONG THE DIFFERENT MODELS

The results obtained for the cases of (2) (with the different definitions), (5), and (6) have been summarized in Table II. For each case, two values are provided. The value in plain text refers to the numerical solution of (4), while the value in italics has been computed by using the best least-squares fit of the numerical function $g(\Delta T)$ in (2) with the Lognormal distribution.

TABLE II
PREDICTED LIFETIMES FOR BOTH MODELS AND ALL DEFINITIONS.
THE LIFETIME IS EXPRESSED IN TERMS OF NUMBER OF POSSIBLE
MISSION PROFILES (LOGNORMAL FIT IN ITALIC)

Model	Predicted Lifetime
Lin. accumul. of the cyclic fatigue	
definition A raw data	9'000-*12'000*
definition A truncated	10'000-*12'000*
definition A filtered	10'000-*11'000*
definition B raw data	102'000-*167'000*
definition B filtered	97'000-*129'000*
definition C raw data	9'000-*13'000*
definition D raw data	19'000-*28'000*
definition E	26'000-*37'000*
Thermo-mechanical model	36'000

Furthermore, the function h has been assumed to be Coffin–Manson-like [1], i.e.,

$$N_f(\Delta T) = 9.10^7 (\Delta T)^{-1.53}.$$ (11)

VIII. DISCUSSION

A. Modeling by Linear Accumulation of the Cyclic Fatigue Damage

The assumption of the linear accumulation of the cyclic fatigue damage returns predicted lifetimes, which are included between 9 000 and 167 000 mission profiles. The use of Definition A predicts a lifetime, which is about one order of magnitude lower than that with Definition B. Definitions A and C return lifetimes in the same range and represent the lowest values in Table II. The lifetime from Definition D is included between those of Definitions A and B. Data truncation and filtration do not affect the lifetime prediction. However, processed data can be fitted with analytical distributions more easily. This is due to the suppression of the low-swing tails, which is not significant in producing thermomechanical damage. The use of the approximation for Δ in the case of Definition D (see Section II-A) reverts in a lifetime, which exceeds by about 25% the value obtained by the exact computation. This approximated procedure simplifies the computation of the correction factor and does not require knowledge of the Coffin–Manson parameters a and q in (2).

B. New Lifetime Prediction Model Based on the Creep Behavior of the Solder Layer

This model provides a lifetime which is closer to that predicted by Definition D in previous case. In spite of its apparent complexity, the model based on creep behavior is robust and returns lifetimes which are not strongly dependent on the uncertainty of the assumed parameters. Furthermore, the lifetime can be easily extrapolated by standard numerical procedures.

IX. CONCLUSION

We have compared the lifetimes predicted by a new thermomechanical model with those predicted by the traditional approach, which assumes the linear accumulation of the thermal cycling fatigue damage. Various definitions of thermal excursion have been introduced. Definition D delivers a lifetime which is very close to that computed by the new thermomechanical model. The main limitation of the new model consists of the fact that (like the Coffin–Manson approach) it fails in predicting the decrease of the module lifetime when it is operated at higher average temperatures. This is due to the assumption that creep is the only plastic deformation mechanism which leads to thermal cycling damage. More complicated models can be developed which take into account additional mechanisms, such as, for instance, stress relaxation, anisotropic effects, and microstructural changes. Unfortunately, the number of free parameters associated with these approaches would make the calibration of those models virtually impossible.

ACKNOWLEDGMENT

REFERENCES

[1] M. Ciappa and W. Fichtner, "Lifetime prediction of IGBT modules for traction applications," in *IEEE Int. Reliability Physics Symp.*, vol. 38, 2000, pp. 210–216.

[2] M. Ciappa, F. Carbognani, P. Cova, and W. Fichtner, "A novel thermomechanics-based lifetime prediction model for cycle fatigue failure mechanisms in power semiconductors," *Microelectron. Reliabil.*, vol. 42, pp. 1653–1658, 2002.

[3] A. Schubert, H. Walter, R. Dudek, B. Michel, G. Lefranc, J. Otto, and G. Mitic, "Thermomechanical properties and creep deformation of lead-containing and lead-free solders," in *Proc. 34th Int. Symp. Microelectronics (IMAPS 2001)*, Baltimore, MD, Oct. 2001.

[4] D. Rubesa, *Lifetime Prediction and Constitutive Modeling for Creep-Fatigue Interaction.* Berlin, Germany: Borntraeger, 1991.

[5] C. Yun, P. Malberti, M. Ciappa, and W. Fichtner, "Thermal component model for electrothermal analysis of IGBT module systems," *IEEE Trans. Adv. Packag.*, vol. 24, pp. 401–406, Aug. 2001.

[6] M. Ciappa, *Some Reliability Aspects of IGBT Modules for High-Power Applications.* Konstanz, Germany: Hartung-Gorre, 2001.

Mauro Ciappa (M'87–SM'96) received the M.S. degree in physics from the University of Zürich, Switzerland, and the Ph.D. degree in engineering sciences from the Swiss Federal Institute of Technology (ETH), Zürich.

He joined the Reliability Laboratory of the ETH in 1986, where he was Head of the Failure Analysis and Reliability Physics Laboratory and Lecturer for reliability physics and failure analysis techniques until 1997. Since 1998, he has been a member of the Integrated Systems Laboratory of the ETH, where he is in charge of physical characterization of semiconductor devices and is Lecturer for Smart Power devices. He has published more than 50 papers in the fields of reliability physics, two-dimensional dopant profiling, and thermal management of power devices. He is co-editor of a monograph on electron and optical beam testing.

Dr. Ciappa has been awarded the IEEE Third Millennium Medal for his contributions to the field of reliability physics.

Flavio Carbognani was born in Parma, Italy, in 1977. He studied telecommunication engineering at the University of Parma. In 2002, he received the M.S. degree from the Swiss Federal Institute of Technology (ETH), Zürich, with a thesis on lifetime prediction models of power semiconductor devices. He is currently working toward the Ph.D. degree at the Integrated Systems Institute (IIS), ETH.

His primary research interest is low-power design, focused on hearing aid applications.

Wolfgang Fichtner (M'79–SM'84–F'90) received the Dipl.Ing. degree in physics and the Ph.D. degree in electrical engineering from the Technical University of Vienna, Vienna, Austria, in 1974 and 1978, respectively.

From 1975 to 1978, he was an Assistant Professor in the Department of Electrical Engineering, Technical University of Vienna. From 1979 to 1985, he was with AT&T Bell Laboratories, Murray Hill, NJ. Since 1985, he has been Professor and Head of the Integrated Systems Laboratory, Swiss Federal Institute of Technology (ETH), Zürich. In 1993, he founded ISE Integrated Systems Engineering AG, a company in the field of technology CAD. Since 1999, he has been Head of the Department of Electrical Engineering, ETH Zürich.

Dr. Fichtner received the IEEE Andy S. Grove Award in 2000. He is a member of the Swiss National Academy of Engineering, and corresponding member of the Austrian National Academy of Science.